

# Audible acoustics from low-magnitude fluid-induced earthquakes in Finland

Oliver D. Lamb<sup>1,\*</sup>, Jonathan M. Lees<sup>1</sup>, Peter E. Malin<sup>2,3</sup>, and Tero Saarno<sup>4</sup>

<sup>1</sup>Department of Geological Sciences, University of North Carolina at Chapel Hill, Chapel Hill, NC, USA

<sup>2</sup>Earth and Ocean Sciences, Nicholas School of the Environment, Duke University, Durham, NC, USA

<sup>3</sup>ASIR Advanced Seismic Instrumentation and Research, Dallas, TX, USA

<sup>4</sup>St1 Deep Heat Oy, Helsinki, Finland

\*olamb@email.unc.edu

## ABSTRACT

Earthquakes are frequently accompanied by public reports of audible low-frequency noises. In 2018, public reports of booms or thunder-like noises were linked to induced earthquakes during a Engineered Geothermal System project in the Helsinki Metropolitan area. In response, two microphone arrays were deployed to record and study these acoustic signals while stimulation at the drill site continued. During the 11 day deployment, we find 39 earthquakes accompanied by recognizable atmospheric acoustic signals. Moment magnitudes of these events ranged from -0.07 to 1.87 with located depths of 4.8 to 6.5 km. Analysis of the largest event revealed a broadband frequency content, including in the audible range, and high apparent velocities across the arrays. We conclude that the audible noises were generated by local ground reverberation during the arrival of seismic body waves. The inclusion of acoustic monitoring at future geothermal development projects will be beneficial for studying seismic-to-acoustic coupling during sequences of induced earthquakes.

---

**This manuscript is a preprint** and was submitted for publication in *Scientific Reports* in March 2021. **Please note that this manuscript has not undergone formal peer review, nor has it been formally accepted for publication.** Subsequent versions of this manuscript may have slightly different content. Please feel free to contact Oliver Lamb with your feedback or comments using the email address above.

---

## Introduction

Earthquakes of a wide range of magnitudes are commonly accompanied by reports and/or measurements of atmospheric acoustic waves at various epicentral distances. These waves may have frequencies ranging from infrasonic (<20 Hz) up to and beyond the minimum limit of human hearing ability (20 - 70 Hz). Cases of the latter have been described as low rumbling sounds or booms<sup>1</sup>, and have been reported for shallow (<2 km) earthquakes in the USA<sup>2</sup> and France<sup>3-5</sup>. The event magnitudes associated with these sounds have been stated to be as low as -2 and -0.7, respectively. Audible noises are also frequently reported for larger magnitude earthquakes, and accompanied by the frequent detection of infrasonic acoustic waves at global distances<sup>6-14</sup>. Mapping of acoustic sources during and immediately after earthquakes has identified three sources of earthquake acoustic signals<sup>15</sup>: i) ‘epicentral’ (i.e. seismic-to-acoustic coupling directly above or near the earthquake epicenter)<sup>6,7</sup>, ii) ‘local’ (i.e. generated by the passage of seismic waves near sensor located at distance from epicenter)<sup>16,17</sup> and iii) ‘secondary’ (i.e. generated by interaction of seismic waves with topographic features)<sup>7,10,18,19</sup>. ‘Epicentral’ acoustic signals have been attributed primarily to vertically propagating body waves (particularly P- and SV-waves) coupling directly into the atmosphere through ground motion at the Earth’s surface<sup>20</sup>. Seismo-acoustic recordings of earthquake acoustic signals at local or epicentral distances are limited to only a few studies<sup>4,19,20</sup>. Here we describe a case study of epicentral acoustic waves generated by earthquakes during a hydraulic stimulation project in Finland, one of the first documented recordings of acoustic signals from an induced earthquake sequence and are amongst the lowest magnitude events to be recorded.

## 36 St1 Deep Heat Oy Venture

37 The Engineered Geothermal System (EGS) pilot project, operated by the St1 Deep Heat Oy energy company, was located in the  
 38 Helsinki Metropolitan area within the campus of Aalto University (Fig. 1). The aim of the project was to develop an EGS  
 39 facility in order to produce a sustainable baseload for the local district heating system<sup>21</sup>. In 2018, a 6.1 km deep stimulation  
 40 well was drilled into crystalline Precambrian Svecofennian basement rocks consisting of granites, pegmatites, gneisses, and  
 41 amphibolites<sup>21</sup>. This bedrock features extensive faults, lineaments, and fractures<sup>22</sup> and is only locally covered by a thin (<10  
 42 m) layer of glacial till or soil<sup>23</sup>. From 4 June to 22 July 2018, a total of 18,160 m<sup>3</sup> of water was pumped into the stimulation  
 43 well at depths of 5.7 to 6.1 km; this included moving injection intervals and multiple stoppages for a few days<sup>21,23</sup>. Induced  
 44 seismicity was monitored by an extensive seismic network, including 3-component borehole seismometers installed in 0.3 to  
 45 1.15 km deep wells at distances up to 8.2 km from the drill site (Fig. 1). The purpose of the seismic network was to provide  
 46 accurate hypocenter locations and magnitudes of induced earthquakes for both industrial and regulatory purposes (i.e. Traffic  
 47 Light System)<sup>21,24</sup>.

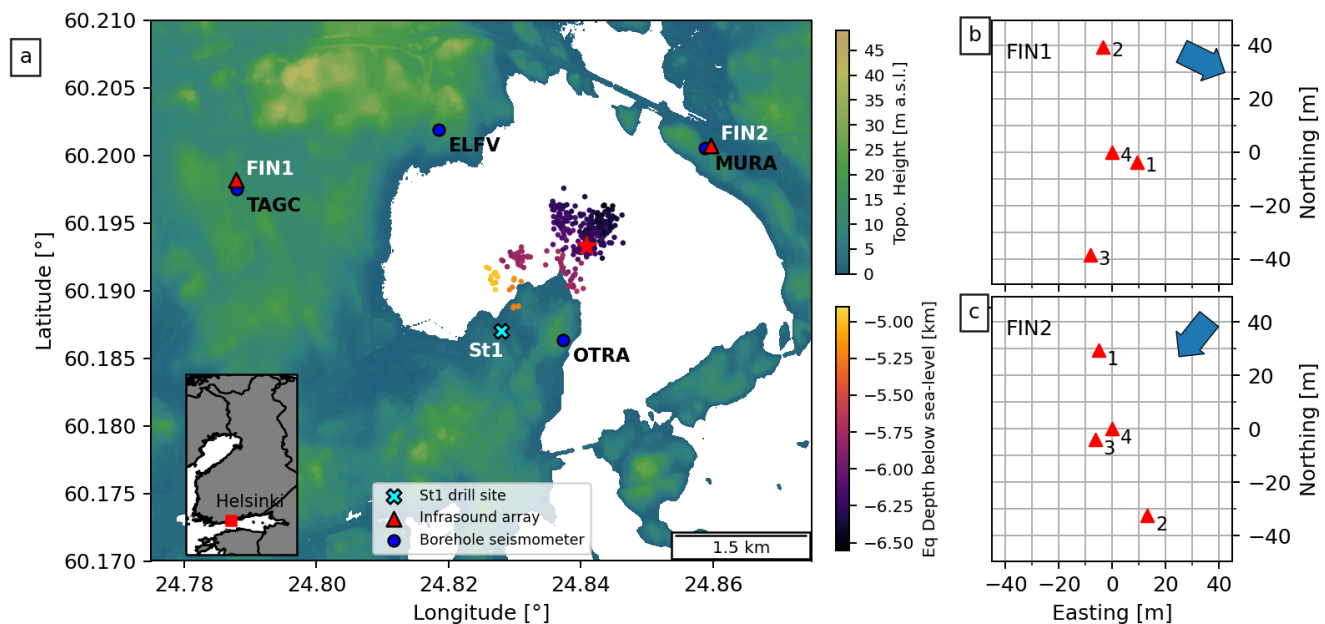


**Figure 1.** (a) Topographic map of the region around the St1 drill site (cyan cross) showing locations and names of borehole seismic stations (blue circles) and temporary acoustic arrays (red triangles). Also plotted are locations of earthquakes recorded during the acoustic deployment, colored by depth. Red star indicates the location of the  $M_w$  1.87 event. Inset: Map of Finland showing location of the Helsinki Metropolitan area. Panels (b) and (c) show the infrasound sensor distribution for arrays FIN1 and FIN2, respectively, with back azimuth direction to the ST1 drill site indicated by the blue arrow.

48 From 4 June to 1 August 2018, a total of 8412 earthquakes were automatically recorded by the network out of which 1977  
 49 were suitable for relocations and magnitude calculations<sup>21</sup>. These events were located across three distinct clusters ranging  
 50 in depths of 4.8 – 6.6 km and moment magnitudes ( $M_w$ ) of -0.76 to 1.86 (Fig. S1 in Supporting Information). Fault plane  
 51 solutions for a set of selected events indicated reverse faulting along pre-existing fractures associated with NW-SE trending  
 52 fault zones reactivated by the hydraulic injection<sup>23,25</sup>. Propagation directions of SH waves across local seismic arrays show  
 53 deviations from the earthquake back azimuths that may be related to the local heterogeneous seismic structure<sup>26</sup>. The Institute  
 54 of Seismology at the University of Helsinki (ISUH) collected 220 public reports of felt earthquakes, which unexpectedly also  
 55 included dozens of audible disturbances, typically described as thunder- or blast-like<sup>23,24</sup>. The largest and most reported event  
 56 was a  $M_w$  1.87 event on 8 July 2018 located at 6.3 km depth (Fig. 1). This event generated 78 public reports and was apparently  
 57 heard up to 9 km away from the epicenter<sup>23</sup>. Notably, spatial distributions of the reports were strongly correlated with the SH  
 58 radiation pattern of the reverse faulting mechanism in the event<sup>23</sup>.

## 59 Data and Methods

60 In response to the reports of audible earthquake events, we deployed two temporary arrays of infrasound microphones in the  
 61 area from 7 – 18 July to study the nature of these atmospheric acoustic signals. The arrays were deployed at distances of  $\sim 2.5$

62 and  $\sim 2.2$  km from the St1 drill site. Each deployment consisted of three microphones extended on cables up to 35 m from  
63 a central data recorder, where a fourth microphone was located (Fig. 1b, c). The data recorder was a REFTEK RT 130 data  
64 logger which provided a 24-bit, GPS-time synchronized recording set to 100 samples per second, resulting in an anti-aliasing  
65 Finite Impulse Response (FIR) filter cut off of 40 Hz. The microphones were identical infraBSU (vers1) microphones, which  
66 incorporate a MEMS sensor and capillary filters to provide a flat response at  $>0.1$  Hz<sup>27</sup>. To aid analysis and interpretation of  
67 acoustic data in this study, we also included seismic data from borehole seismometers located near each array (TAGC and  
68 MURA; Fig. 1a). Each seismometer was composed of a three-component Sunfull PSH geophone sensor ( $f_N = 4.5$  Hz) recording  
69 at 500 samples per second and located  $\sim 1.15$  km below the surface (For more information, see Kwiatek et al. 2019<sup>21</sup>).

70 For this study, all data were filtered with a 2 Hz high-pass Butterworth filter to reduce continuous background noise (unless  
71 otherwise indicated). Data were manually inspected for consistent arrivals across at least two microphones in each array to  
72 assess if earthquake-generated atmospheric acoustic waves were detected following an induced earthquake. To estimate the  
73 arrival times for different body wave phases at each array, we use P- and S-wave velocities of 6.25 and 3.75 km.s<sup>-1</sup> respectively,  
74 as estimated from borehole logs at the St1 drill site (see supplementary materials in Kwiatek et al. 2019<sup>21</sup>). One of the  
75 key advantages of deploying acoustic microphones in an array configuration is it permits the calculation of back azimuth  
76 direction and slowness of acoustic waves propagating across the deployment. Back azimuth is calculated using least-squares  
77 beamforming where time delays between sensors are calculated using cross-correlation<sup>28</sup>. Here we estimated back azimuths  
78 and slowness values for 0.5 s windows with 90% overlap within the first 3 s after the initiation time of the earthquake. Windows  
79 in which calculated slowness exceeded physically possible values (i.e.  $>4$  s.km<sup>-1</sup>) or relative power was lower than 0.6 were  
80 discarded. Relative power is defined as the signal power of the mean waveform for peak slowness divided by average element  
81 power in the same time window. We used waveform envelopes, determined from the square root of the Hilbert Transform,  
82 which were then smoothed using the average of an 8 sample moving window (Fig. 4a, b). All analysis presented here was  
83 carried out within the ObsPy python package<sup>29</sup>.

## 84 Observations

85 During 7 – 18 July, 266 earthquakes were detected and relocated within a few hundred metres of the stimulation interval. These  
86 events occurred at depths of 4.8 to 6.5 km below sea level and had moment magnitudes ranging from -0.19 to 1.87 (Fig. 1a,  
87 2a, b). Of the 266 earthquakes, 39 were followed shortly by atmospheric disturbances across at least one array that may be  
88 interpreted as earthquake associated acoustic waves (Fig. 2). Atmospheric disturbances were more commonly seen at FIN2  
89 ( $n=36$ ) than FIN1 ( $n=9$ ), with only 3 events seen exclusively at the latter. The smallest event was a  $M_w$  -0.07 on 8 July, and the  
90 largest was the widely heard  $M_w$  1.87 on the same day (Fig. 2c). As the latter earthquake produced the highest signal-to-noise  
91 ratios at both microphone arrays, the remainder of this section will focus on the analysis of acoustic data from this particular  
92 event.

93 For the  $M_w$  1.87 event the acoustic data recorded at FIN2 have peak amplitudes an order of magnitude larger than those  
94 recorded at FIN1 (Fig. 3c, g). Frequency spectra highlight the broadband nature of the atmospheric acoustic signals, with  
95 frequencies ranging from 2 to 40 Hz (Fig. 3d, h), which are the limits set by the filter and sampling rates (see Section ). The  
96 acoustic waves and their spectra at each array appear to show distinct multi-phase arrivals that correlate with seismic waves  
97 recorded at the nearby borehole seismometers (Fig. 3a, b, e, f). The different arrival phases at each array appear to be coincident  
98 with the predicted arrivals of P- and S-waves (dotted and dashed red lines in Fig. 3). The highest acoustic amplitudes are  
99 correlated with the arrival of the S-waves at each array. Calculated values of back azimuth and slowness at or near the estimated  
100 time of arrivals for P- and S-waves (red lines in Fig. 4a, b) indicate arrivals from the direction of the  $M_w$  1.87 event epicenter  
101 (Fig. 4c, d). Slowness values at these times indicate relatively initially high propagation velocities across the array, which  
102 rapidly decrease to lower values in the subsequent time windows (Fig. 4e, f).

## 103 Discussion

104 Here we have presented evidence for infrasonic and audible atmospheric acoustic signals generated by low magnitude fluid-  
105 induced earthquakes. These observations are notable for two reasons: i) these are the first recorded earthquake-generated  
106 acoustic signals from induced earthquakes, and ii) they represent the lowest magnitude events to be recorded by acoustic  
107 microphones. (There are reports of audible noises from earthquakes with magnitudes as low as -2<sup>5</sup> but these events were not  
108 recorded with microphones.) Manual inspection of data identified at least 39 events where acoustic waves were recorded  
109 propagating across at least one array of sensors (Fig. 2). This represents only 15% of all earthquakes relocated during the  
110 deployment, but the location of the arrays within a large metropolitan area with a large number of noise sources may have  
111 acted to reduce this proportion. The acoustic waves contained broadband frequency ranges from 2 up to 40 Hz, and possibly  
112 higher but is limited by the anti-alias FIR filter of the sample recording rate (Fig. 3d, h). This frequency range overlaps with the  
113 lower range of human hearing (down to 20 Hz), therefore confirming that thunder- or blast-like sounds heard by the public

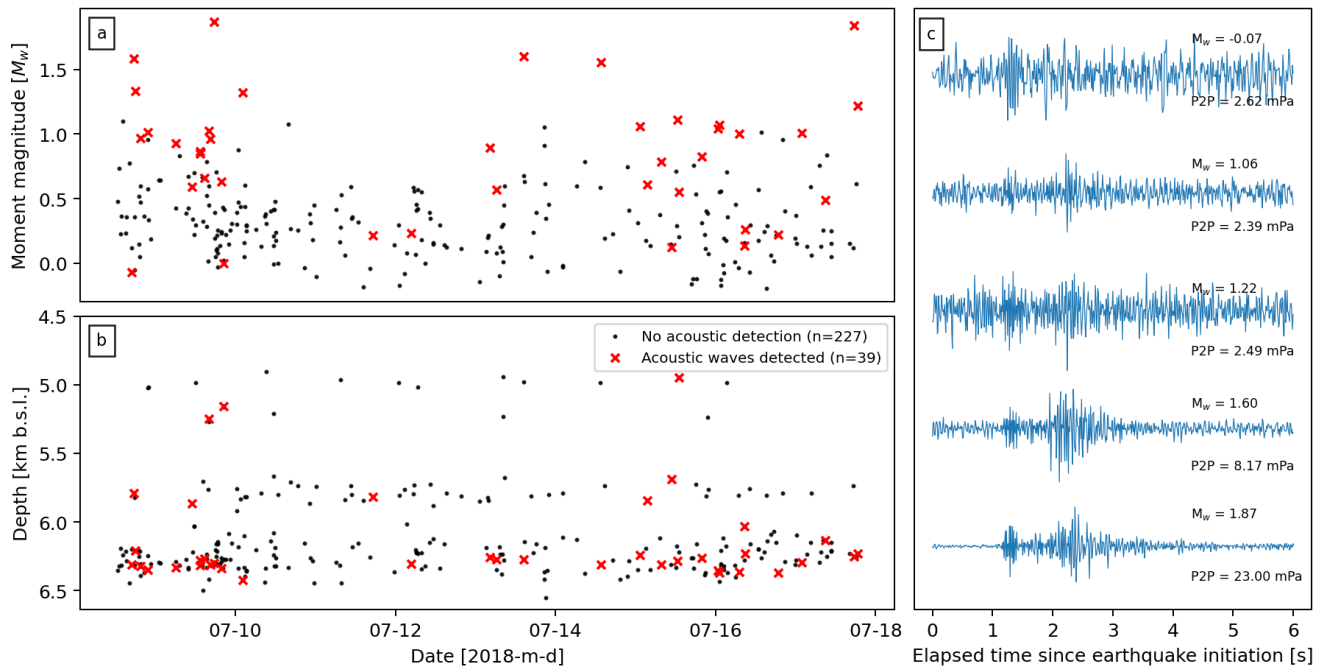


**Figure 2.** Moment magnitudes (a) and depths (b) of the 266 relocated seismic events recorded during the infrasound array deployment near the St1 Deep Heat Oy EGS project. Red 'x' indicate the events which were detected by at least one acoustic array. (c) 6 s of normalised acoustic data (highpass filtered at 5 Hz) recorded by sensor 2 at FIN2 after the initiation of five example earthquakes, including the lowest and highest magnitude events. Calculated  $M_w$  and recorded peak-to-peak pressure amplitudes (P2P) of each event is indicated on the right; each event was located at 6.2 to 6.3 km depth. (See figures S2 to S11 in Supporting Information for waveforms and frequency spectrograms from all microphones for each event.)

114 were generated by the earthquakes<sup>23,24</sup>. These frequency ranges also match previously reported values from audible natural  
 115 earthquakes<sup>4,20</sup>.

116 During the expected arrival times of the P- and S-waves at each array the back azimuth values align at or around the direction  
 117 of the earthquake epicenter (Fig. 4c, d). It is notable that a significant number of windows were discarded due to unrealistic  
 118 slowness values or low relative power. This is likely due to low signal-to-noise ratios as well as poor array-perpendicular  
 119 slowness resolution due to the narrow deployment configuration of the arrays. Ideally, 3 or 4 microphone sensor arrays would  
 120 be arranged as an equilateral triangle. However, the geometry of each array here was forced by the limited availability of  
 121 deployment areas which is to be expected for a rapid response deployment in an urban environment. Nevertheless, azimuthal  
 122 resolution is expected to be good and poor for bearings perpendicular and parallel to the arrays, respectively. The consistent  
 123 deviation between calculated back azimuths and great-circle direction to the earthquake epicenter at FIN2 (Fig. 4d) may be  
 124 related to either: 1) the non-optimal array configuration or 2) the locally heterogeneous seismic structure. The latter was  
 125 inferred to explain similar deviations at local seismic arrays deployed in the same region during the same induced seismic  
 126 sequence<sup>26</sup>.

127 Calculated slowness values during the arrival of seismic waves begin with relatively high propagation velocities across the  
 128 array, but rapidly decrease to lower values (Fig. 4e, f). The initially low slowness values correlate with waves of either high  
 129 velocities ( $>1 \text{ km}\cdot\text{s}^{-1}$ ) or near-vertical wave arrival directions at the array. Considering the ratio between earthquake depths (4.8  
 130 – 6.5 km) and epicenter-array distances ( $<2.5 \text{ km}$ ), it is reasonable to expect near vertical arrival angles of seismic waves at each  
 131 array. The higher slowness values in the subsequent windows indicate lower propagation velocities on the same magnitude as  
 132 atmospheric acoustic waves. This can be interpreted as 'secondary infrasound' from sources in close proximity to the arrays  
 133 ( $<150 \text{ m}$ ), within the same back azimuth from source to receiver. However, slowness resolution perpendicular to the arrays is  
 134 likely to be poor due to the forced narrow deployment configuration. Nevertheless, the atmospheric acoustic signals recorded  
 135 during the largest earthquake, and all other recorded events, were likely generated by ground motion at and near the station  
 136 during and immediately after the arrival of P- and S-waves at the ground surface within close proximity of the microphone  
 137 arrays.

138 A notable observation from the public reports compiled during the induced earthquake sequence is the geographical  
 139 distribution of disturbances correlated with the radiation patterns of S-waves (See Fig. 5 in Hillers et al. 2020<sup>23</sup>). The FIN2

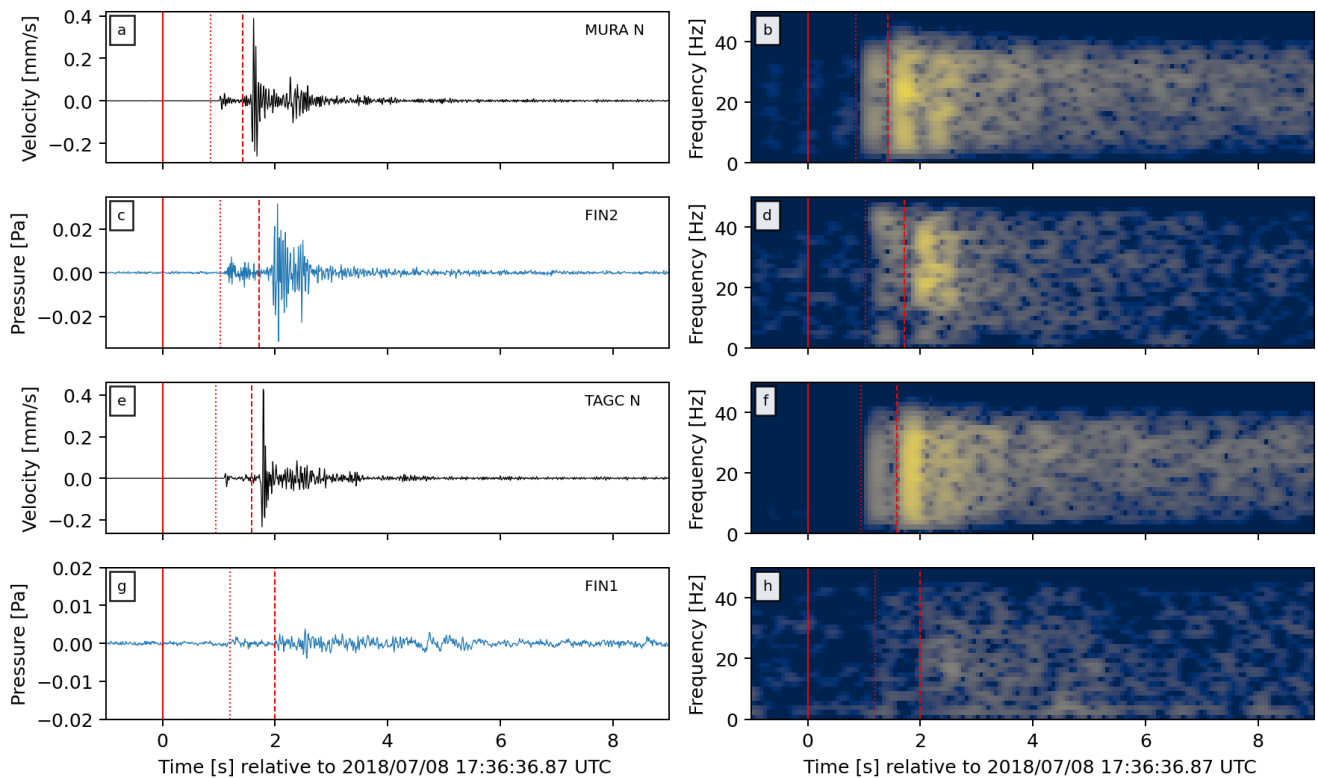


**Figure 3.** Filtered waveforms (left column) and their respective frequency spectrograms (right column) of the  $M_w$  1.86 event as recorded by seismic station MURA (a, b), acoustic array FIN2 (c,d), seismic station TAGC (e, f) and acoustic array FIN1 (g, h). Note that the seismic waveforms are from the north component of the station. Spectrograms were calculated with 0.5 s windows with 90% overlap. Also plotted is the time of the event (solid red line), as well as predicted arrival times for P- and S-wave phases (dotted and dashed red lines, respectively) from source locations to each station or array.

140 acoustic array was located adjacent to the area with the greatest number of reports. This pattern correlates with the amplitude  
 141 difference between the acoustic waves recorded at FIN1 and FIN2 for the  $M_w$  1.86 event, with amplitudes an order of magnitude  
 142 higher at the latter than the former (Fig. 3c, d). Furthermore, a higher number of earthquake-generated acoustic waves were  
 143 recorded at FIN2 (N=36) than at FIN1 (N=9). Another factor to consider is that the FIN1 array was deployed on the margin of  
 144 an active golf course which was built on top of a former municipal waste landfill, while FIN2 was deployed in an area where  
 145 buildings are frequently constructed directly onto outcropping bedrock. This suggests that the presence of a soft sedimentary  
 146 layer above the bedrock may act as a dampener during seismic-to-acoustic coupling of body waves. Previous observations have  
 147 suggested that low frequency (<10 Hz) signals in the coda of acoustic waves may be generated by Rayleigh waves in a thin  
 148 (<100 m) sedimentary layer above the bedrock<sup>4</sup>. No such low frequency coda is evident in the recordings seen here (Fig. 3d, h).  
 149 The correlation between public sound report distributions and the acoustic amplitudes highlights the potential utility of such  
 150 reports for monitoring at future EGS projects, particularly when high-quality geophysical recordings may not be available.

151 Given that the infrasound sensors are typically placed in direct contact with the ground surface during deployments,  
 152 contamination of recorded infrasound signals by physical shaking of the sensor could be a concern. However, testing of the  
 153 seismic response of various acoustic sensors have consistently concluded that physical vibration does not significantly influence  
 154 the recorded infrasound signals<sup>4,20,30</sup>. The MEMS-based microphones used in this study (InfraBSU vers1) have low inertial  
 155 mass and are similar in design to the MEMS-based transducers described in Marcillo et al. 2012<sup>27</sup>. These sensors were found  
 156 to have minimal seismic-to-noise coupling during calibration studies at the Facility for Acceptance, Calibration and Testing site  
 157 at the Sandia National Laboratories<sup>19</sup>. Therefore, we do not consider direct seismic shaking of the sensor to be of importance in  
 158 the acoustic signals presented here.

159 A common observation in previous earthquake acoustic studies is the presence of secondary infrasound generated away  
 160 from the earthquake epicenter<sup>7,9,10,15,18,19</sup>. These acoustic signals are confirmed to be caused by the interaction of surface  
 161 waves with topography or other significant crustal features<sup>10,15</sup>. These are usually manifested as an unusually long coda of  
 162 secondary arrivals after the local infrasound phases<sup>19</sup>. The infrasound waves described here have relatively short durations

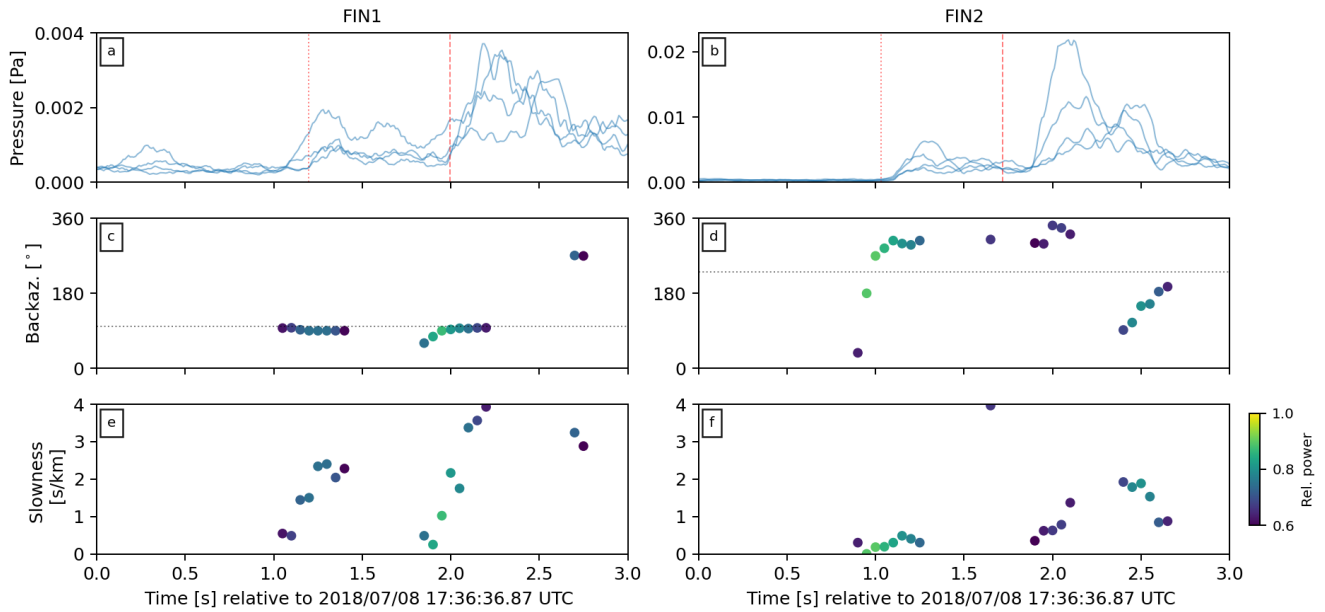


**Figure 4.** Beamforming results for arrays FIN1 (left column) and FIN2 (right column) for the first 3 seconds after the  $M_w$  1.86 event. (a, b) Smoothed waveform envelopes from each element in each array. Dotted and dashed lines plot the estimated arrival times of P- and S-waves, respectively (from epicentre to array). (c, d) Back azimuth calculations for 0.5 s moving windows with 90% overlap. Horizontal dotted lines plot the azimuth from each array to the  $M_w$  1.86 event epicenter. (e, f) Calculated slowness values across each array for each 0.5 s window. Points in panels c-f are colored by relative power, where lighter colors indicate higher relative power.

163 with no significant coda, therefore we infer that no secondary infrasound has been generated by the induced earthquakes. We  
 164 interpret this as a result of the low magnitudes of the events, as well as the lack of steep topographical features around the St1  
 165 drill site (Fig. 1a). However, due to the location within an metropolitan area, we cannot rule out the presence of acoustic signals  
 166 generated by mechanical shaking of buildings or other structures (e.g. bridges) near each array. Altogether, we interpret the  
 167 signals presented here as ‘local’ earthquake acoustic signals generated by ground surface reverberation during the direct arrival  
 168 of body waves generated by fluid-induced earthquakes.

## 169 Conclusions

170 Acoustic monitoring can help explain human observations and may also provide quantitative insights into the mechanics  
 171 of ground motions responsible for generating earthquake sounds. Here we have presented acoustic events recorded within  
 172 the Helsinki Metropolitan area in July 2018 during hydraulic stimulation at a pilot Engineered Geothermal System project.  
 173 Based on the estimated timing of body wave arrivals, frequency content of the waveforms, as well as estimated slowness  
 174 calculations, we have interpreted these acoustic events as being generated by reverberation of the ground surface during the  
 175 arrival of P- and S-waves from induced low magnitude earthquakes. Although only a minor proportion of induced earthquakes  
 176 generated recognizable acoustic waves, events with moment magnitudes ranging from -0.07 to 1.87 were recorded with acoustic  
 177 microphones at the surface. As far as we are aware, these events represent the first induced earthquakes and are amongst the  
 178 lowest magnitude events to be recorded with acoustic microphones. Given that Traffic Light Systems are increasingly being  
 179 implemented to reduce the potential seismic hazard due to induced seismicity<sup>24</sup>, and the considerable public interest generated  
 180 by audible earthquakes in the Helsinki Metropolitan area<sup>23,24</sup>, future projects for developing geothermal systems can benefit  
 181 from deploying acoustic sensors to provide more detailed information in responses to public concern.

## 182 References

- 183 1. Michael, A. J. *Earthquake Sounds*, 1–5. Encyclopedia of Earth Sciences Series (Springer International Publishing, 2019).
- 184 2. Ebel, J. E., Vudler, V. & Celata, M. The 1981 microearthquake swarm near Moodus, Connecticut. *Geophys. Res. Lett.* **9**,  
 185 397–400, DOI: [10.1029/GL009i004p00397](https://doi.org/10.1029/GL009i004p00397) (1982).
- 186 3. Sylvander, M. & Mogos, D. G. The sounds of small earthquakes: Quantitative results from a study of regional macroseismic  
 187 bulletins. *Bull. Seismol. Soc. Am.* **95**, 1510–1515, DOI: [10.1785/0120040197](https://doi.org/10.1785/0120040197) (2005).

- 188 4. Sylvander, M., Ponsolles, C., Benahmed, S. & Fels, J. F. Seismoacoustic recordings of small earthquakes in the Pyrenees:  
189 Experimental results. *Bull. Seismol. Soc. Am.* **97**, 294–304, DOI: [10.1785/0120060009](https://doi.org/10.1785/0120060009) (2007).
- 190 5. Thouvenot, F., Jenatton, L. & Gratier, J.-P. 200-m-deep earthquake swarm in Tricastin (lower Rhône Valley, France)  
191 accounts for noisy seismicity over past centuries. *Terra Nova* **21**, 203–210, DOI: [10.1111/j.1365-3121.2009.00875.x](https://doi.org/10.1111/j.1365-3121.2009.00875.x)  
192 (2009).
- 193 6. Mikumo, T. Atmospheric pressure waves and tectonic deformation associated with the Alaskan earthquake of March 28,  
194 1964. *J. Geophys. Res.* **73**, 2009–2025, DOI: [10.1029/JB073i006p02009](https://doi.org/10.1029/JB073i006p02009) (1968).
- 195 7. Young, J. & Greene, G. Anomalous infrasound generated by the Alaskan earthquake of 28 March 1964. *The J. Acoust. Soc.*  
196 *Am.* **71**, 334–339, DOI: [10.1121/1.387457](https://doi.org/10.1121/1.387457) (1982).
- 197 8. Olson, J. V., Wilson, C. R. & Hansen, R. A. Infrasound associated with the 2002 Denali fault earthquake, Alaska. *Geophys.*  
198 *Res. Lett.* **30**, DOI: [10.1029/2003GL018568](https://doi.org/10.1029/2003GL018568) (2003).
- 199 9. Le Pichon, A., Guilbert, J., Vallée, M., Dessa, J. X. & Ulziibat, M. Infrasonic imaging of the Kunlun Mountains for the  
200 great 2001 China earthquake. *Geophys. Res. Lett.* **30**, DOI: [10.1029/2003GL017581](https://doi.org/10.1029/2003GL017581) (2003).
- 201 10. Mutschlechner, J. P. & Whitaker, R. W. Infrasound from earthquakes. *J. Geophys. Res.* **110**, 1–11, DOI: [10.1029/2004JD005067](https://doi.org/10.1029/2004JD005067) (2005).
- 203 11. Le Pichon, A., Mialle, P., Guilbert, J. & Vergoz, J. Multistation infrasonic observations of the Chilean earthquake of 2005  
204 June 13. *Geophys. J. Int.* **167**, 838–844, DOI: [10.1111/j.1365-246X.2006.03190.x](https://doi.org/10.1111/j.1365-246X.2006.03190.x) (2006).
- 205 12. Arrowsmith, S. J. *et al.* A seismoacoustic study of the 2011 January 3 Circleville earthquake. *Geophys. J. Int.* **189**,  
206 1148–1158, DOI: [10.1111/j.1365-246X.2012.05420.x](https://doi.org/10.1111/j.1365-246X.2012.05420.x) (2012).
- 207 13. Pilger, C. *et al.* Infrasound and seismoacoustic signatures of the 28 September 2018 Sulawesi super-shear earthquake. *Nat.*  
208 *Hazards Earth Syst. Sci.* **19**, 2811–2825, DOI: [10.5194/nhess-19-2811-2019](https://doi.org/10.5194/nhess-19-2811-2019) (2019).
- 209 14. Shani-Kadmiel, S., Averbuch, G., Smets, P., Assink, J. & Evers, L. The 2010 Haiti earthquake revisited: An acoustic  
210 intensity map from remote atmospheric infrasound observations. *Earth Planet. Sci. Lett.* **560**, 1–11, DOI: [10.1016/j.epsl.2021.116795](https://doi.org/10.1016/j.epsl.2021.116795) (2021).
- 212 15. Arrowsmith, S. J., Johnson, J. B., Drob, D. P. & Hedlin, M. A. The seismoacoustic wavefield: A new paradigm in studying  
213 geophysical phenomena. *Rev. Geophys.* **48**, 1–23, DOI: [10.1029/2010RG000335](https://doi.org/10.1029/2010RG000335) (2010).
- 214 16. Cook, R. K. Infrasound radiated during the montana earthquake of 1959 august 18. *Geophys. J. Royal Astron. Soc.* **26**,  
215 191–198, DOI: [10.1111/j.1365-246X.1971.tb03393.x](https://doi.org/10.1111/j.1365-246X.1971.tb03393.x) (1971).
- 216 17. Kim, T. S., Hayward, C. & Stump. Local infrasound signals from the tokachi-oki earthquake. *Geophys. Res. Lett.* **31**,  
217 L20605, DOI: [10.1029/2004GL021178](https://doi.org/10.1029/2004GL021178) (2004).
- 218 18. Shani-Kadmiel, S., Assink, J. D., Smets, P. S. M. & Evers, L. G. Seismoacoustic Coupled Signals From Earthquakes  
219 in Central Italy: Epicentral and Secondary Sources of Infrasound. *Geophys. Res. Lett.* **45**, 427–435, DOI: [10.1002/2017GL076125](https://doi.org/10.1002/2017GL076125) (2018).
- 221 19. Johnson, J. B., Mikesell, T. D., Anderson, J. F. & Liberty, L. M. Mapping the sources of proximal earthquake infrasound.  
222 *Geophys. Res. Lett.* **47**, 19, DOI: [10.1029/2020GL091421](https://doi.org/10.1029/2020GL091421) (2020).
- 223 20. Hill, D. P., Fischer, F. G., Lahr, K. M. & Coakley, J. M. Earthquake sounds generated by body-wave ground motion. *Bull.*  
224 *Seismol. Soc. Am.* **66**, 1159–1172 (1976).
- 225 21. Kwiątek, G. *et al.* Controlling fluid-induced seismicity during a 6.1-km-deep geothermal stimulation in Finland. *Sci. Adv.*  
226 **5**, DOI: [10.1126/sciadv.aav7224](https://doi.org/10.1126/sciadv.aav7224) (2019).
- 227 22. Elminen, T. *et al.* Fault structures in the Helsinki area, southern Finland. *Geol. Surv. Finland Special Pap.* **47**, 185–213  
228 (2008).
- 229 23. Hillers, G. *et al.* The 2018 Geothermal Reservoir Stimulation in Espoo/Helsinki, Southern Finland: Seismic Network  
230 Anatomy and Data Features. *Seismol. Res. Lett.* DOI: [10.1785/0220190253](https://doi.org/10.1785/0220190253) (2020).
- 231 24. Ader, T. *et al.* Design and implementation of a traffic light system for deep geothermal well stimulation in Finland. *J.*  
232 *Seismol.* **24**, 991–1014, DOI: [10.1007/s10950-019-09853-y](https://doi.org/10.1007/s10950-019-09853-y) (2020).
- 233 25. Leonhardt, M. *et al.* Seismicity during and after stimulation of a 6.1 km deep enhanced geothermal system in Helsinki,  
234 Finland. *Solid Earth* **12**, 581–594, DOI: [10.5194/se-12-581-2021](https://doi.org/10.5194/se-12-581-2021) (2021).

- 235 **26.** Taylor, G., Hillers, G. & Vuorinen, T. A. T. Using Array-Derived Rotational Motion to Obtain Local Wave Propagation  
236 Properties From Earthquakes Induced by the 2018 Geothermal Stimulation in Finland. *Geophys. Res. Lett.* **48**, DOI:  
237 [10.1029/2020GL090403](https://doi.org/10.1029/2020GL090403) (2021).
- 238 **27.** Marcillo, O., Johnson, J. B. & Hart, D. Implementation, characterization, and evaluation of an inexpensive low-power low-  
239 noise infrasound sensor based on a micromachined differential pressure transducer and a mechanical filter. *J. Atmospheric*  
240 *Ocean. Technol.* **29**, 1275–1284, DOI: [10.1175/JTECH-D-11-00101.1](https://doi.org/10.1175/JTECH-D-11-00101.1) (2012).
- 241 **28.** Olson, J. V. & Szuberla, C. A. *Processing Infrasonic Array Data*, 1487–1496 (Springer New York, 2008).
- 242 **29.** Krischer, L. *et al.* ObsPy: a bridge for seismology into the scientific Python ecosystem. *Comput. Sci. & Discov.* **8**, 1–17,  
243 DOI: [10.1088/1749-4699/8/1/014003](https://doi.org/10.1088/1749-4699/8/1/014003) (2015).
- 244 **30.** Bedard, A. J. Seismic Response of Infrasonic Microphones. *J. Res. Natl. Bureau Standards - C. Eng. Instrumentation* **75C**,  
245 41–45 (1971).

## 246 **Acknowledgements**

247 The authors wish to thank Dr Peter Leary and the technicians at the St1 Deep Heat project for their help and logistical support  
248 during the acoustic sensor deployment. This research was performed while ODL held an NRC Research Associateship with  
249 the U.S. Army Research Laboratory/Army Research Office while based at the University of North Carolina at Chapel Hill.  
250 All acoustic data presented here will be made available, without undue reservation, to any qualified researcher. Data from the  
251 borehole seismometers were transmitted to the Institute of Seismology at the University of Helsinki as part of a regulatory  
252 agreement with the city of Espoo and have not been released to the public. Topographic data used in Fig. 1a were downloaded  
253 from the National Land Survey of Finland via the Open data file download service (last accessed December 2020).

## 254 **Author contributions statement**

255 All authors conceived the experiment, OL conducted the experiment and analysed the data. All authors reviewed and discussed  
256 the results, and reviewed the manuscript.

## 257 **Additional information**

### 258 **Competing interests**

259 The authors declare no competing interests.